Proceedings of the 21st ICSMGE, Vienna, Austria, 14 – 19 June 2026. Pistrol, Adam & Schweiger (eds.)
Published by: ÖGG, Austrian Society for Geomechanics, Salzburg, Austria, ISBN 978-3-9503898-4-5
https://doi.org/10.53243/ICSMGE2026-871

A 3D numerical case study of Sprayed Concrete Lining tunnel construction beneath an existing building

Jiaming Liu, Aikaterini Tsiampousi, David Taborda
Imperial College London, London, United Kingdom, j.liu22@imperial.ac.uk

Agustin Ruiz López
Seequent - The Bentley Subsurface Company, Delft, The Netherlands; Imperial College London, London, United Kingdom

ABSTRACT: The potential impact of tunnelling on the serviceability of existing infrastructures must be carefully considered before construction. 3D Finite Element (FE) analysis has proved to be a useful method when predicting the impact of tunnelling superstructures. Compared with 2D FE analysis, it enables the step-by-step tunnel construction process to be simulated, as well as geometries along the direction of tunnelling to be considered realistically. To minimize ground movements, large diameter Sprayed Concrete Lining (SCL) tunnels are commonly constructed through a sequence where a smaller pilot tunnel is excavated first, followed by the enlargement of the pilot tunnel into the full-size tunnel. Such construction process, not typically investigated with 3D FE analysis, is considered in this paper with the simulation of the construction of the Elizabeth Line through a site near Whitechapel station in London, UK. This location provides an interesting case study because the surface settlements of both a greenfield section and of a three-storey building were monitored during construction. The greenfield section was simulated first to gain an understanding of how the construction sequence, various soil properties and tunnel lining stiffness affected the obtained ground movements. The section including the building was investigated subsequently with an emphasis on the evolution of the ground surface settlement with the advancement of tunnel excavation, as well as on the influence of the pilot-enlargement tunnel construction sequence. The results are in good agreement with the field measurements. Moreover, it is highlighted that during enlargement, bending of the existing pilot tunnel lining in sections yet to be enlarged occurs, which in turn affects how the ground surface settlement develops. This investigation demonstrates that the interaction mechanisms between pilot and enlargement tunnels are complex and that considering the detailed construction sequence is essential to capture the movements of the ground and superstructures in numerical analysis.

KEYWORDS: 3D Finite Element Analysis, pilot tunnel, enlargement, step-by-step construction sequence, ground surface settlement.

1 INTRODUCTION

The impact of tunnel-induced ground movements on the serviceability of existing superstructures has been widely discussed over the past decades. Finite Element (FE) analysis is often adopted to predict such impact. 2D FE analysis has the advantage of being easy to set up and of relatively short calculation times. Moreover, its reliability has been proven through extensive research. However, there are still certain aspects of tunnelling that it fails to capture. Firstly, 2D analysis fails to incorporate the step-by-step nature of the tunnel excavation process and how the advancement of the tunnel impacts progressively the superstructures above. Secondly, large diameter SCL tunnels are commonly constructed through a sequence where a small pilot tunnel is excavated first and subsequently enlarged into the final diameter to reduce ground movement. In practice, the timeline for these two operations normally overlap to reduce time and cost. 2D FE analysis, however, can only simulate it in a separated manner, i.e., the enlargement phase only starts after the pilot tunnel construction finishes. Thirdly, when considering tunnel-building interaction using 2D FE analysis, the out-of-plane dimension of the building cannot be adequately considered.

With all the limitations described above, 3D FE analysis is required to simulate accurately tunnel-building interaction problems. This paper is based on a case study in the Whitechapel area involving the construction of the Elizabeth Line, using field data first to calibrate the numerical model based on the results of a greenfield section, and then to validate simulation results for the building section. Emphasis has been placed on how the ongoing tunnelling process influences ground longitudinal settlement development and how the interaction between the constructed pilot tunnel lining and the enlargement excavation could influence ground movement.

2 3D FINITE ELEMENT ANALYSIS

2.1 *Geometry*

Figure 1. Plan view of Whitechapel Station area and layout of surrounding buildings.

The site consists of Vallance Road Gardens and a building nearby supported by a piled raft foundation along Castlemaine Street, highlighted by a green square and a blue rectangle in Figure 1. The ground profile found at this site is a typical London geology profile, with 3.7 m thick Made Ground, 3 m River Terrace Gravel, 27.3 m London Clay, 9.7 m Lambeth Group Clay, 10 m Lambeth Group Sand, and 9.9 m Thanet Sands. The Chalk bedrock underneath is set as the bottom boundary of the FE model. The vertical boundary is set to be 100 m away from the tunnel axis. PLAXIS 3D v2024.2 (Seequent, 2024) is used in all the analyses presented in this paper.

2.2 *Soil properties and initial stresses*

Made Ground is modelled as linear elastic-perfectly plastic with a Mohr-Coulomb failure criterion. The other layers are all modelled using a non-associated perfectly plastic Mohr-Coulomb failure criterion combined with an isotropic nonlinear stiffness model developed by Taborda et al. (2016) and

Table 1. Basic soil properties.

Material	Unit Weight, γ (kN/m^3)	Effective cohesion, c' (kPa)	Effective angle of shearing resistance, φ'	Angle of dilation, ψ	Drained-Young's modulus, E' (kPa)	Poisson's ratio, μ
Made ground	19	0	30	0	10000	0.25
River Terrace Gravel	20	0	35	17.5	Non-linear	
London Clay	20	5	25	12.5	Non-linear	
Lambeth Clay	20	25	27	13.5	Non-linear	
Lambeth Sand	20	0	34	17	Non-linear	
Thanet Sands	20	0	40	20	Non-linear	

Table 2. Nonlinear stiffness properties adopted assuming p'_{ref}=100 kPa (Gawecka et al., 2017).

Material	G_{ref} (kPa)	m_G	a	b	$R_{G,min}$	G_{min} (kPa)
River Terrace Gravel	41939.6	1.0	0.000145	1.00	0.03511	3000
London Clay (Run 1)	51743.5	1.0	0.000056	0.90	0.06450	2667
Lambeth Group Clay	51924.5	1.0	0.000110	0.95	0.04662	2667
Lambeth Group Sand	81346.3	1.0	0.000015	1.00	0.14557	1000
Thanet Sands	65275.2	1.0	0.000046	0.85	0.02631	2000
Material	K_{ref} (kPa)	m_K	r	s	$R_{K,min}$	K_{min} (kPa)
River Terrace Gravel	49843.1	1.0	0.000247	1.25	0.15440	3000
London Clay (Run 1)	26692.7	1.0	0.000127	1.80	0.13275	5000
Lambeth Group Clay	61331.7	1.0	0.000065	1.40	0.07589	5000
Lambeth Group Sand	49843.1	1.0	0.000026	0.90	0.08377	5000
Thanet Sands	29813.5	1.0	0.000155	1.10	0.27947	5000

Table 3. Nonlinear stiffness properties adopted for London Clay Run 2 and 3 assuming p'_{ref}=100 kPa (Jurecic et al., 2013).

Material	G_{ref} (kPa)	m_G	a	b	$R_{G,min}$	G_{min} (kPa)
London Clay (Run 2)	16653.8	1.0	0.000787	1.12	0.11325	2667
London Clay (Run 3)	41394.5	1.0	0.000064	1.11	0.06418	2667
Material	K_{ref} (kPa)	m_K	r	s	$R_{K,min}$	K_{min} (kPa)
London Clay (Run 2)	21400.7	1.0	0.000139	2.10	0.13531	5000
London Clay (Run 3)	21400.7	1.0	0.000139	2.10	0.13531	5000

implemented into PLAXIS as a user-defined model by Taborda et al. (2023a and b).

The basic soil properties adopted are summarized in Table 1 above, while Table 2 summarizes the nonlinear stiffness properties (Gawecka et al., 2017). The coefficient of earth pressure, K_0, is taken as 0.5 for the Made Ground and River Terrace Gravel. For London Clay, K_0 is equal to 1.5 for the top 10 m, linearly reducing to 1.0 for the next 10 m, remaining 1.0 below this point, including all other layers below London Clay, a variation which is based on the profile described in Schroeder et al. (2004).

This site, where the ground surface is at 13.4 mOD, has a perched aquifer above the London Clay, with the water table found to be at 8 mOD, and a bottom aquifer in the Thanet Sands with the pressure head at -27 mOD, as indicated in the Crossrail Groundwater Monitoring Report (Geotechnical Consulting Group, 2011), shown as Figure 2.

2.3 *Tunnel modelling*

Three major tunnels are passing under this site, which are the Running Tunnel East (RTE), Crossover tunnel (XOV) and the Launch Chamber West tunnel (LCW) (Figure 1). All three tunnels are SCL tunnels and constructed through the pilot and enlargement sequence. To study the pilot-enlargement interaction without interference from other tunnels, only RTE tunnel is considered in this 3D FE analysis, as it is the first tunnel constructed at this site. The pilot tunnel has 6.2 m diameter and 250 mm thick lining, while the final tunnel diameter is 9.12 m with 350 mm thick lining. The tunnel is located 29.3 m below ground level.

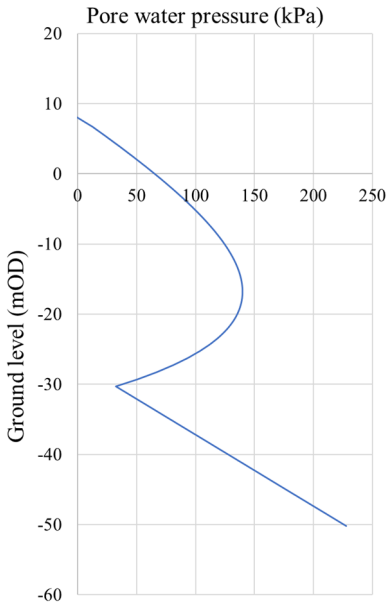

Figure 2. Pore water pressure profile.

2.4 *Building simulation*

The superstructure is simulated with the following components: a plate element with an equivalent building stiffness, solid elements representing the concrete foundation slab, beam elements representing the piles, and a line load and two point-

loads representing all loads of the building acting on the foundation slab and the two side walls, respectively.

The building is a 3-storey structure located near Vallance Road Gardens which is 86 m long, 10 m wide, and 10.5 m high. The equivalent building stiffness is calculated using the parallel axis theorem assuming the neutral axis located at mid-height of the building (Franzius et al., 2004).

Several assumptions are made to calculate building loads. The floor slabs are taken as 0.3 m thick, and the material for them is assumed as reinforced concrete with the unit weight of 25 kN/m^3 . The façade of the building is assumed to be made of 0.3 m thickness bricks with unit weight of 20.8 kN/m^3. The live load acting on the building is assumed as 1.5 kN/m^2 while the weight of the roof is taken as 0.85 kN/m^2.

The piles are 18.5 m long with 4 m spacing and a diameter of 0.5 m.

3 GREENFIELD CONDITIONS

In the 3D greenfield model only half the domain was included taking advantage of symmetry. The tunnel was constructed with a slice-by-slice excavation manner where a 1 m length slice of unsupported soil was excavated each time, with the tunnel lining being installed on the previously excavated slice at the same time. Only the pilot excavation phase was considered here. This model was validated against field data and a parametric study aimed at understanding the influence of different aspects of the model was carried out: model length in the tunnel longitudinal direction, London Clay properties, coefficient of earth pressure profile and stiffness of the tunnel lining.

3.1 *Model length*

In 2D FE analysis, tunnels are considered as having infinite length in the out-of-plane direction. However, when modelling tunnels in 3D, it is important to consider an adequate length of the tunnel in order to minimize boundary effects. Therefore, three tunnel lengths of 10, 15 and 20 times the tunnel diameter are considered. The settlement trough is taken at the central section of the model and shown in Figure 3.

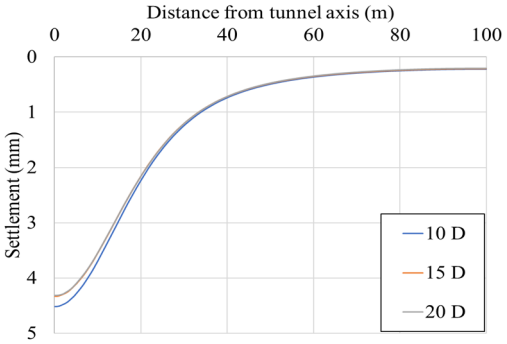

Figure 3. Ground surface settlement trough from the central of the model.

The cases with 20 D and 15 D lengths give slightly smaller settlement when compared with the 10 D length. Considering the calculation time, which naturally increases with model length, the 15 D model length is adopted in all subsequent analyses.

3.2 *London Clay properties*

There has been a variety of model formulations and parameters adopted to capture the nonlinear response of London Clay (Jardine et al., 1986; Taborda et al., 2016). In addition, laboratory testing has yielded inconclusive trends in terms of nonlinear stiffness of London Clay for samples retrieved from various sites (Gawecka et al., 2017; Jurecic et al., 2013). Therefore, three sets of parameters to capture London Clay stiffness from recent research were adopted to study their influence: one provided by Gawecka et al. (2017) (Run 1, shown in Table 2), one converted from data measured at Heathrow Terminal 5 (Jurecic et al., 2013) (Run 2, Table 3), and one converted from the lower bound from previous commercial experiments (Jurecic et al., 2013) (Run 3, Table 3).

Figure 4 shows the variations of normalized shear modulus with axial strain in the undrained triaxial test for the three sets of parameters considered. Figure 5 compares the corresponding settlement troughs in comparison with field data.

Run 1 has the overall largest stiffness in Figure 4 and naturally it produces the smallest settlement in Figure 5. As for Run 2 and Run 3, the latter exhibits a larger stiffness at small strain levels, with Run 2 becoming stiffer than Run 3 as strain levels increase. Considering that tunnel construction typically produces strains significantly larger than 0.01% (Mair, 1993), it is the operational stiffness at these strain levels that is of importance when examining the results. Therefore, in Figure 5, Run 3 gives much bigger settlement than Run 2. Given the greater proximity to field data, Run 3 is considered to give the best simulation result, with these parameters being used henceforth.

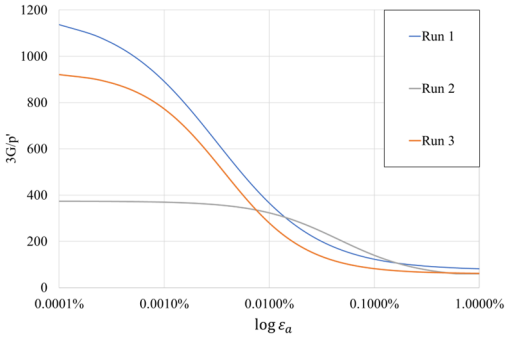

Figure 4. Normalized tangent shear stiffness of London Clay.

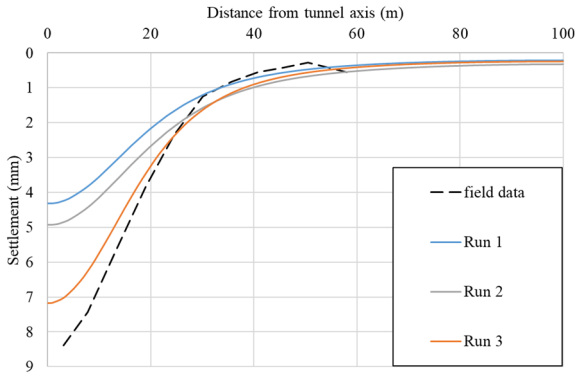

Figure 5. Settlement trough with different small-strain stiffness behaviors of LC.

3.3 *Tunnel lining stiffness*

The tunnel lining construction for this site adopted the Sprayed Concrete Lining (SCL) method. Sprayed Concrete stiffness develops nonlinearly over time after the construction, requiring a time-dependent material model. To study how much this aspect influences the ground movement prediction, two cases are considered: a stiffness developing over time, and a fully developed concrete stiffness with an upper bound value of 30 GPa. To model the first case, the nonlinear development of shotcrete stiffness is simplified into the step varying process

shown in Figure 6, where stiffness changes every 7 days. The blue line shows the original variation (Dubasaru, 2013) while the orange line denotes the adopted simplification. Table 4 lists the corresponding values of Young's modulus.

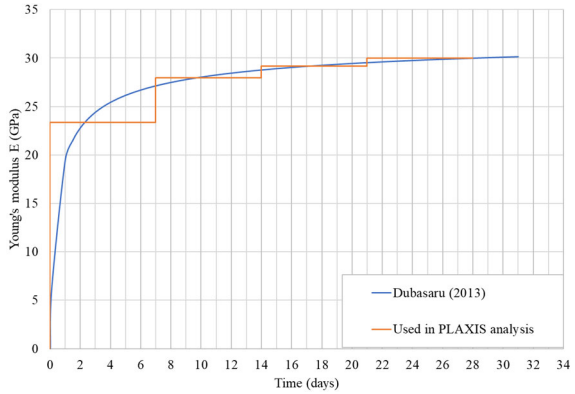

Figure 6. Increase of sprayed concrete stiffness with time.

Table 4. Tunnel lining stiffness adopted in the analysis.

Time (days)	Young's modulus E (GPa)
0-7	23.34
8-14	27.96
15-21	29.16
22-28	30

The settlement troughs given by the two-tunnel lining stiffnesses adopted are shown in Figure 7. Clearly, step-varying lining stiffness has a limited influence on the final result when compared to the 30 GPa lining stiffness case. Therefore, a constant stiffness of 30 GPa was adopted in all further analyses.

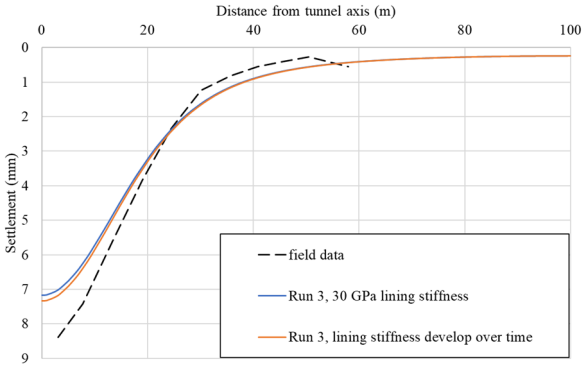

Figure 7. Settlement trough with different tunnel lining stiffness (London Clay properties adopted Run 3).

3.4 *Coefficient of earth pressure profile*

The profile of coefficient of earth pressure at-rest (K_0) is very sensitive to the site's stress history. Therefore, considerable differences exist in proposed values of K_0 between different sites (Hight et al., 2007). Given this, three profiles are considered in this study, as shown in Figure 8. Profile 1 is the same as the one mentioned in Schroeder et al. (2004), while Profiles 2 and 3 only differ by changing the value in the top 10 m of London Clay from 1.5 to 1.25 and 1.1, respectively.

Figure 9 shows the settlement results adopting these different K_0 profiles combined with the London Clay properties associated with Run 3 and a tunnel lining stiffness of 30 GPa. While smaller K_0 leads to bigger settlements, overall, the K_0 profile variation has very limited impact on the ground movements. This is likely due to the tunnel being located at greater depths within the London Clay where the values of K_0 are very close to 1.0 for the three profiles, as shown in Figure 8. However, the influence of the K_0 profile may be more significant for building settlement supported by pile foundations, and this relationship requires further investigation. K_0 profile 1 was adopted in all the following analyses.

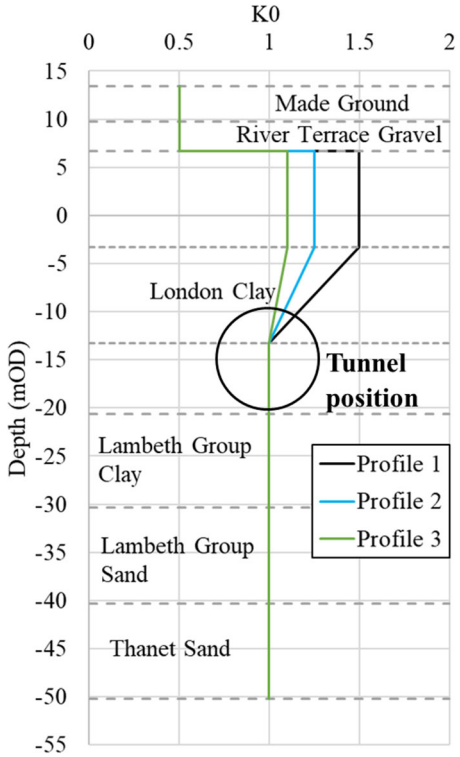

Figure 8. Three K_0 profiles adopted.

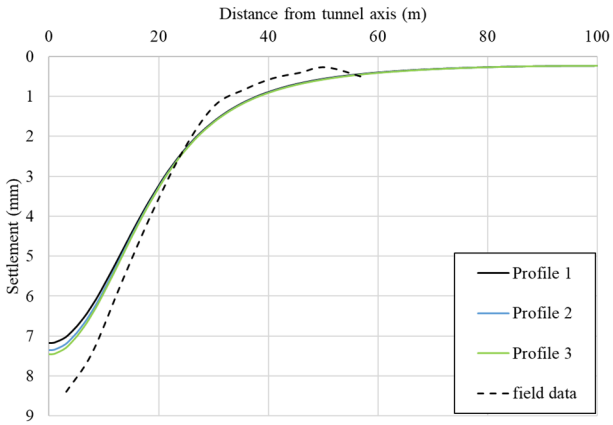

Figure 9. Settlement trough with different K_0 profiles.

4 TUNNEL-BUILDING INTERACTION

Based on the above calibration of parameters with greenfield data, a 3D FE model is set up with a piled building on top and both RTE tunnel pilot and enlargement excavation sequence considered. The model has a length of 15 D in the tunnel excavation direction. The London Clay adopts the Run 3 set of parameters, a Young's Modulus of 30 GPa for the tunnel lining and profile 1 for K_0 (Figure 8).

4.1 *Tunnel construction sequence*

The tunnel construction sequence is shown in Table 5, where "Adv" refers to 1 m length advancement over the whole cross-section of the pilot tunnel. With reference to the enlargement tunnel, the following process is simulated: 2 m length advancement at the crown, simulated in two separate phases of the analysis with 1 m length each, followed by 2 m length advancement of the invert in a subsequent, single phase, i.e.

every 2 m length full face tunnel enlargement excavation is simulated in three phases.

Table 5. RTE tunnel construction sequence.

	Pilot	Enlargement
Stage 1	adv 1 – adv 24	
Stage 2	hold	adv 1 – adv 17
Stage 3	adv 25- adv 36	adv 18 – adv 29
Stage 4	adv 37-98	Hold
Stage 5	hold	adv 30 – adv 64
Stage 6	adv 99 – adv 108	adv 65 – adv 134
Stage 7	adv 109 – finish	Hold
Stage 8		adv 135 – finish

4.2 *Result verification*

First, the simulation result is compared with field data to further examine the appropriateness of the previously chosen previous parameters choice, shown in Figure 10. It is important to note that, because of the interaction between pilot and enlargement tunnel construction phases, it is difficult to isolate the settlements caused by pilot or enlargement only.

In Figure 10, "pilot" refers to the end of Stage 4 (see Table 5) where enlargement is on hold, while a large proportion of the pilot tunnel has already been excavated. "Enlargement" refers to the end of Stage 8 and includes the overall settlement resulting from the impact of both pilot and enlargement excavations. In the pilot stage, there is a 5 mm difference between the results of the simulation and the field data. However, after the enlargement of the tunnel, the final prediction of settlement shows a very good agreement with field data for both the maximum settlement and the settlement trough shape, suggesting that overall, the assumptions made in the numerical simulation were reasonable.

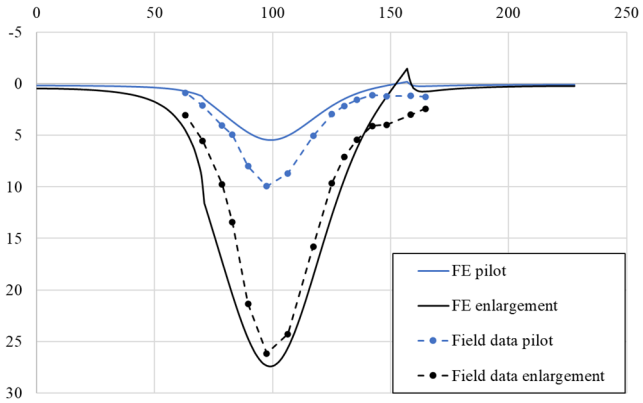

Figure 10. 3D building cross section ground surface settlement comparing with field data.

4.3 *Pilot-enlargement interaction effect*

Figure 11 shows the evolution of the longitudinal (tunnel axis direction) ground surface settlement directly above the tunnel axis (i.e. maximum settlement) obtained in the 3D FE analysis. In addition to the standard tunnel lining stiffness of 30 GPa (solid lines), the results obtained with a lower bound tunnel stiffness value of 7 GPa (broken lines) are also shown for the discussion later on.

The figure shows a clear development of longitudinal ground surface settlement as the pilot and enlargement excavation progress. It is worth noticing that, from stage 1 to stage 2, and from stage 4 to stage 5, when the pilot excavation face is stationary while the enlargement excavation face is progressing, a small reduction in settlement appears near to the pilot tunnel excavation face, which seems counterintuitive as one would expect further settlements as the tunnel excavation progresses. The observed reduction in settlement might be related to the contribution of the already installed pilot tunnel lining. A plausible mechanism is explained in the following.

With the enlargement of the excavation, the soil tends to move into the unsupported void, applying additional pressure to the existing pilot tunnel lining in its vicinity. Such pressure takes the form of an overall downward force acting on the pilot tunnel lining, which acts like a hollow beam, producing deformations similar to those shown in red in Figure 12: the far end rises slightly as the enlargement side moves downwards. This causes the ground surface to have a similar settlement shape.

Furthermore, from stage 3 to stage 4 and from stage 6 to stage 7, where the enlargement excavation is on hold and the pilot tunnel excavation keeps progressing, the evolution of settlements at the surface suggests an obvious bending deformation in the mid span of the installed pilot lining.

Similarly, this can also be explained by the installed pilot tunnel lining acting as a beam embedded in the soil, as shown schematically in Figure 13. At the tunnel excavation face, the soil tends to move towards the unsupported void, therefore the installed pilot tunnel lining takes a downward force causing it to bend.

In Figure 11, the influence of tunnel lining stiffness to the evolution of the longitudinal ground surface settlement can also be observed from the results obtained with a lining stiffness of 7 GPa. For the 7 GPa lining, the settlements are generally larger than that with the 30 GPa lining, as expected. Additionally, the settlement reduction caused by the enlargement excavation becomes smaller, see stages 1 versus 2, and 4 versus 5 with broken lines. Moreover, the biggest deflection ratio at the hogging zone (maximum relative settlement divided by hogging zone length) becomes smaller when adopting a softer tunnel lining stiffness. For the 30 GPa lining, the maximum hogging deflection ratios at stages 4 and 7 are calculated to be 1.31E-4 m/m and 1.55E-4 m/m. With a 7 GPa lining, these values reduce to 1.20E-4 m/m and 1.45E-4 m/m, respectively. This indicates smaller bending deformation for the softer tunnel lining. In soil–structure interaction, a softer lining mobilizes lower pressures acting on the lining during excavation-induced stress redistribution, which, therefore, reduces bending deformation in the lining.

The longitudinal ground settlement trough progressing with the tunnel excavation demonstrated the interaction effect between the installed pilot tunnel lining and the enlargement section. This interaction appears to slightly reduce ground surface settlement, although further investigation is required to establish whether this mechanism is present in field structures.

5 CONCLUSIONS

Based on field data gathered at the Whitechapel area in London, detailed 3D FE analyses were conducted of the construction of a tunnel for the Elizabeth Line. First, a greenfield model is set up to study the impact of model length, London Clay properties, tunnel lining stiffness and coefficient of earth pressure profile on the prediction of ground surface settlement trough. Subsequently, a case with superstructure was set up. The cross-sectional settlement trough showed a good agreement with field data. The settlement trough in the longitudinal direction was also plotted for different stages during tunnel construction. A trend was observed where the installed pilot tunnel lining behaved in a similar way to a beam. Soil unloading caused by new excavation led to an increase in the pressure applied to the installed lining, influencing the ground surface settlement shape. Further investigation is needed to establish whether such mechanism manifests itself in monitored structures.

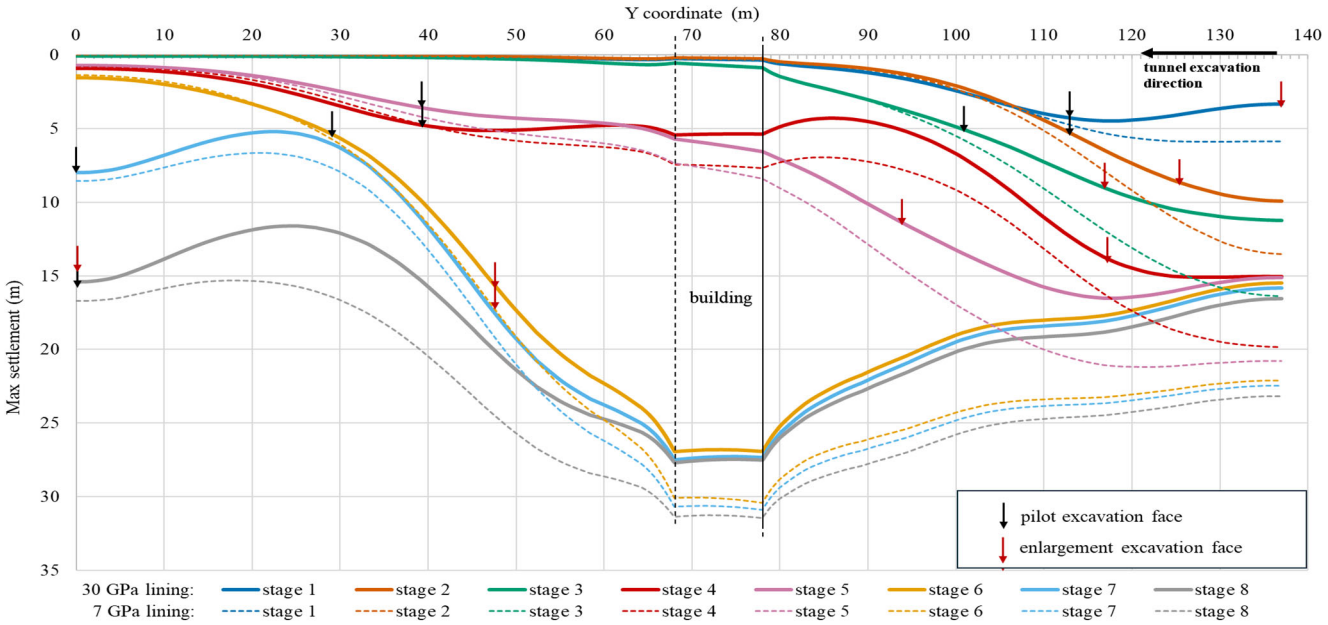

Figure 11. Longitudinal direction ground surface settlement of different tunnel excavation stages.

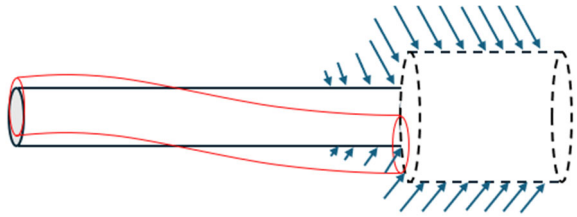

Figure 12. Enlargement excavation and existing pilot tunnel lining interaction mechanism (schematic diagram does not represent real deformation magnitude).

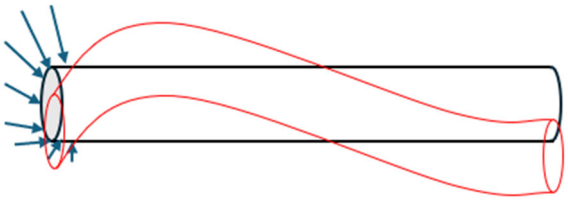

Figure 13. Installed pilot lining bending deformation caused by tunnel excavation (schematic diagram does not represent real deformation magnitude).

6 REFERENCES

Dubasaru, V. 2013. Pile clash mitigation. *MSc thesis*. Imperial College London.

Franzius, J. N., Potts, D. M., Addenbrooke, T. I., and Burland, J. B. 2004. The influence of building weight on tunnelling-induced ground and building deformation. *Soils and Foundations* 44(1), 25-38.

Gawecka, K. A., Taborda, D. M. G., Potts, D. M., Cui, W., Zdravković, L., and Haji Kasri, M. S. 2017. Numerical modelling of thermo-active piles in London Clay. *Proceedings of the Institution of Civil Engineers - Geotechnical Engineering* 170(3), 201-219.

Geotechnical Consulting Group, 2011. *Engineering Groundwater Level Monitoring – December 2011, Report No. CRL1-GCG-C2-RAN-CRG03-00002, Rev. 2.0.* Crossrail Limited.

Hight, D. W., Gasparre, A., Nishimura, S., Minh, N. A., Jardine, R. J., and Coop, M. R. 2007. Characteristics of the London Clay from the Terminal 5 site at Heathrow Airport[J]. *Géotechnique* 57(1), 3-18.

Jardine, R. J., Potts, D. M., Fourie, A. B., and Burland, J. B. 1986. Studies of the influence of non-linear stress–strain characteristics in soil–structure interaction[J]. *Geotechnique* 36(3), 377-396.

Jurečič, N., Zdravković, L., and Jovičić, V. 2013. Predicting ground movements in London Clay. *Proceedings of the Institution of Civil Engineers-Geotechnical Engineering* 166(5), 466-482.

Mair, R. J. 1993. Unwin Memorial Lecture 1992 Developments in Geotechnical Engineering Research: Application to Tunnels and Deep Excavations. *Proceedings of the Institution of Civil Engineers* Civil engineering 97(1), 27–41.

Schroeder, F. C., Potts, D. M., and Addenbrooke, T. I. 2004. The influence of pile group loading on existing tunnels. *Géotechnique* 54, 351-362.

Seequent, 2024. PLAXIS 3D 2024.1 Reference Manual [PDF manual]. Bentley Systems. https://bentleysystems.service-now.com/community?id=kb_article&sysparm_article=KB0108423

Taborda, D. M. G., Potts, D. M., and Zdravković, L. 2016. On the assessment of energy dissipated through hysteresis in finite element analysis. *Computers and Geotechnics* 71, 180-194.

Taborda, D. M. G., Kontoe, S., and Tsiampousi, A. 2023a. *IC MAGE Model 01—strain-hardening/softening Mohr-Coulomb failure criterion with isotropic small strain stiffness (Version 2.0).* Zenodo.

Taborda, D. M. G., Kontoe, S., and Tsiampousi, A. 2023b. *IC MAGE UMIP – universal model interface for PLAXIS (Version 3.3).* Zenodo.